RADII AND EFFECTIVE TEMPERATURES FOR K AND M GIANTS AND SUPERGIANTS. II.

H. M. Dyck
U.S. Naval Observatory, Astrometry Department, Navy Prototype Optical Interferometer, Rural Route 14, Box 447, Flagstaff, Arizona
meldyck@sextans.lowell.edu

G. T. van Belle[1]
Jet Propulsion Laboratory, California Institute of Technology, 4800 Oak Grove Drive, MS306-388, Pasadena, California 91109
gerard@huey.jpl.nasa.gov

R. R. Thompson[1]
Department of Physics and Astronomy, University of Wyoming, Laramie, Wyoming 82071
thompson@sparky.uwyo.edu

ABSTRACT

We present new interferometric observations for 74 luminous red stars, made in the near infrared. We show that our 2.2μm uniform disk diameters agree with other near-infrared diameter determinations (lunar occultations and interferometers) for 22 stars measured in common with ours. From our new data we derive effective temperatures that are compared to our previous work and to comparable observations made by lunar occultations at Kitt Peak. The combined data set yields 91 luminosity II, II-III and III stars that have well-determined spectral types spanning the range from about K0 to about M8 . There are 83 stars in the sample that define an approximately linear relationship between spectral type and effective temperature for giants with a dispersion of 192 K at each spectral type. Eight of the stars have temperatures that are roughly 750K too low for their spectral types. These stars are not known to be at the high luminosity end of the range of stars observed and are not recognized as binary stars. At present we have no explanation for their low effective temperatures. We also show that Hipparcos parallaxes combined with our angular diameters yield linear radii precise enough to see differences in the average radius between luminosity class II and luminosity class III stars.

I. INTRODUCTION

Measurements of the angular diameters for oxygen-rich giants and supergiants at 2.2 μm have been a long-term goal at IOTA (the Infrared Optical Telescope Array) since first fringes were obtained in late 1993. In this paper we report new visibility observations for 74 evolved stars. We felt that it was timely to publish the data so that it would nearly coincide with the release of the parallax data set from Hipparcos. The combination of well-determined angular diameters with distances will lead to a large body of linear diameters for the upper right-hand part of the HR diagram. Although we have a larger body of observations than we report here, we restrict the present discussion to stars with observed average visibility levels $V \leq 0.8$. These stars are well enough resolved that the resulting errors in the effective temperatures are $\sigma_T \leq 300$K.

A complete description of the interferometer may be found in Carleton et al. (1994); the methods used to observe fringes and reduce the fringe data to uniform-disk angular diameters have been described by Dyck et al. (1996), hereafter referred to as Paper I. In Paper I we discussed the advantages of observing at 2.2

[1] NASA Space Grant Fellow

μm, compared to both shorter and longer wavelengths. We will not repeat these discussions here, although we stress that we are generally using the fringe visibility at a single spatial frequency point to determine the uniform-disk (UD) diameter.

This method appears to be sufficiently accurate for giants and supergiants but may lead to errors for Mira variables (see, for example, Tuthill 1994); there are no known Mira variables in the present sample of stars. As an example of the accuracy of this method for characterizing the angular diameter of a star, we show our accumulated data for the M5 supergiant α^1 Her taken at IOTA and IRMA (see Dyck et al. 1993 for the latter) plotted in Figure 1. A simple uniform-disk visibility function, with θ_{UD} = 33.2±0.8 milliarcsec (mas), has been fitted to the data. One may see that there is no systematic departure from the UD function at spatial frequencies lower than the first zero. Beyond the first zero the observed data also fit the UD well although there may be a small amount of excess power (1-2%) that could originate in surface structure such as spots or limb brightening. The quality of the data is not sufficiently high to be able to judge that point at the present time. Because the uniform disk fits this extended-atmosphere supergiant well, we expect that the results for less extended luminosity class III stars will be at least as good. Thus, we feel justified in determining the angular diameter for luminosity I, II and III stars from a single observation of the visibility made at one spatial frequency point. Note also that the comparison of the IRMA and IOTA data, taken at epochs differing by about 4 years, sets a limit on the amount of variability over this timescale.

We have also compared our angular diameter measurements with those taken by other observing methods, including lunar occultations at 1.65 and 2.2μm and interferometry at 2.2μm at CERGA and at IOTA with the FLUOR beam-combination system. The references to these other diameter measurements are White & Feierman (1987) for the occultations, DiBenedetto & Rabbia (1987) and DiBenedetto & Ferluga (1990) for the CERGA observations and Perrin et al. (1997) for the FLUOR data. The comparisons are shown in Figure 2 for the 22 stars measured in common and the agreement is seen to be good. If we fit a line to the data then the IOTA observations differ in slope by 3.8% from the other observations and have an offset at the origin of about -0.6 mas. Note that, compared to IOTA, the lunar occultation technique is a completely different method for obtaining angular diameters, CERGA is a different interferometer with a different method of estimating fringe visibility and FLUOR is the same interferometer but with a different beam combination scheme.

II. THE OBSERVATIONS

The new data are reported in Table 1, where we have given the Bright Star Catalogue (Hoffleit 1982) number, a common name or other identifier, the date of the observation (as year-month-day), the projected interferometer baseline (in m), the visibility and the uniform disk angular diameter (in mas) and an associated error (also in mas). Because the interferometer response is not constant, owing to mechanical changes in the instrument and to atmospheric fluctuations during the night, we calibrate the observations of a science source frequently. We choose calibration sources that are unresolved (visibility amplitude greater than about 95%) and that are placed within about 5 degrees of the science source in the sky. The normal mode of observing is to alternate observations between the science source and the calibrator in a time interval of order 5 minutes to minimize the effects of the atmosphere-instrument variations. Calibrated visibilities are obtained by dividing the observed visibility amplitude of the science source by the observed visibility amplitude of the calibrator, after correction for the estimated calibrator size. As we reported in Paper I, we have assigned an error of ±0.051 to the calibrated visibility measured on a single night, based upon our experience with the scatter in the observed visibility for the same star over different nights; the error is decreased as the square root of the number of nights on which observations were made. This error and the visibility were used to compute the error in the UD diameter.

The referee has pointed out to us that the application of such a naive error estimate to the visibility might not be expected. For example, assuming photon statistics as the principal source of noise, one would expect the error to grow with increasing visibility for a source of fixed brightness. We have applied the error to the full range of visibility measurements. Further, owing to correlations in the two data channels resulting from atmospheric effects it may not be reasonable to assume that using two channels reduces the error by $\sqrt{2}$. We may justify the application of this simple visibility error estimate by considering all the repeated data available from this paper and Paper I, where the maximum baseline variation is no more than 4% among the observations. A random distribution in the projected baseline of ±2% around a mean baseline of 37.5 m produces an rms variation in the observed visibility of ±0.0085 about a mean visibility of 0.55 for a star of angular diameter 8 mas. For all the stars in our program with two or more observations we have computed the mean and the absolute deviation for each observation. These absolute deviations are shown plotted in Figure 3, as a function of the measured visibility, where the entire sample has been used. We note that the upper limit to the deviations is about 0.2 with the bulk of the points lying at levels less than 0.1. In fact, four stars produce the points that deviate most widely from the rest of the sample. Notable among these is RX Boo, for which we reported the largest sample of repeated observations (see Paper I). This was done because we suspected at the time that RX Boo might show some time variability in the measured visibility. If we exclude RX Boo from the sample on the grounds that it may be variable, the rms fluctuation in the remaining stars in the distribution shown is ±0.0526. Subtracting in quadrature the rms variation noted above for the dispersion caused by projected baseline changes from the observed visibility scatter in the sample yields a corrected estimate for the error of ±0.0519. This is very close to the estimate obtained in Paper I made with a smaller data set and indicates that two detector channels are indeed better than one by about the expected factor; we adopt the error from Paper I for consistency. Note also that there is no correlation between the absolute deviation and the observed visibility over the approximate range $0.1 \leq V \leq 0.9$. In particular, there is no growth of error with increasing visibility so that we feel justified in applying a simple error estimate over the entire range of our visibility measurements. The observed distribution indicates only that other sources of error than photon statistics are important to the observations in the near infrared.

In Table 2 we have converted the UD diameters to Rosseland mean diameters, using the relationship $\theta_R = 1.022\theta_{UD}$, adopted from the paper by Scholz & Takeda (1987) (see our Paper I for a discussion). Effective temperatures were computed from these Rosseland mean diameters and bolometric fluxes estimated from broad-band photometry. The photometric data were obtained from the Simbad database where we have used the JP11 measurements when they were available. When photometric data were not available for some wavelengths we filled in by interpolation using mean colors for the observed spectral type. The raw magnitudes were corrected for reddening, using the scheme described in Paper I, and integrated numerically to obtain the bolometric flux. Note that we have not computed effective temperatures for all stars reported in Table 1. Rather, we have restricted the sample to those stars that we judge to have well-determined spectral types; references to the sources for these spectral types are given in Table 2. We also included earlier observations from Paper I, bringing the total number of stars with effective temperature estimates to 70. Where there were overlapping data, we have averaged the UD diameters together, weighted by the error.

Random errors in the effective temperatures were computed by assuming an uncertainty of 15% in the bolometric flux (arising from errors in the absolute calibration, errors in the reddening estimate and variability) and the computed error in the UD diameter listed in Table 2. The interested reader should consult

Paper I for details of the error estimates for the bolometric flux.

III. DISCUSSION

1. Effective Temperatures

The effective temperatures for luminosity classes II, II-III and III have been plotted in Figure 4, where we have plotted only those stars for which the error in the temperature was ≤300K. This resulted in 60 stars. We have also included the available occultation data from Ridgway et al. (1980) supplemented by a few additional stars reported in Paper I. The justification for combining the two data sets is based upon the analysis carried out in Paper I. In that paper (see Table 5), we compared the effective temperature scale defined by Ridgway et al. (1980) with the one derived from IOTA interferometry. The result was that the IOTA scale was about 100 K cooler than the occultation scale at spectral type K1III but about 130 K warmer at spectral type M6 III. The intrinsic scatter at each spectral type was estimated to be about 100 K, so it seems reasonable to conclude that the two scales are identical. We have not replotted the stars observed at CERGA since they overlap almost completely with the IOTA observations. The total number of effective temperatures determined from occultation measurements is 31, bringing the total number plotted in Figure 4 to 91 stars. This is nearly 50% more stars than were reported in Paper I.

One may notice three general features in the figure. First, there is a uniform mix of IOTA interferometric and occultation temperatures. Each data set appears to cover the band defined by the other with no systematic separation. This agrees with the conclusions given in Paper I. Second, all but 8 of the stars are concentrated at the upper part of the distribution. The eight discordant stars form a parallel sequence offset by about 750K to cooler temperatures from the average of the remaining 83 stars. Finally, at the scale shown in the figure, there is a linear decrease of temperature over the range of spectral types from G8 to M8.

Because we have mixed together luminosity classes II and III it is of interest to determine whether the eight discordant stars in Figure 4 have luminosities systematically higher than the remainder of the stars. One might anticipate this effect based upon our previous result (Paper I) showing that supergiants have systematically lower temperatures than their giant counterparts at the same spectral type. The eight stars under discussion here are υ Leo, γ^1 Leo, 75 Tau, 6 Leo, 46 Leo, HD75176, FL Ser and Z UMa, all classified as luminosity class III. Two of the eight are known to be members of double systems, which could produce the observed effect, but the other stars appear to be single.

If we assume that the roughly linear relationship between spectral type and effective temperature shown in the figure is, in fact, correct, then we may determine an equation that will describe the temperature over this range of spectral types. A linear regression to all data except the eight discordant stars results in the following

$$T = -106\,ST + 4580\ \mathrm{K},$$

where the index *ST* has possible values -2,..0,..,5,6,..8 corresponding to spectral classes G8,..,K0,..,K5,M0,..M8, respectively. The regression for the 83 stars yields a standard error for a single estimate of temperature of ±192 K. If some other functional form better expresses the relationship between the spectral type and effective temperature for giants, then this error is an upper limit to the average dispersion at each spectral class. We have shown this regression in Figure 4 for comparison to the observed data.

The error in the computed effective temperatures is divided between the uncertainty assumed for the bolometric flux density and the error in the measured angular diameter, with the error in the diameter giving the larger contribution. The mean relative error in the angular diameter for the stars listed in Table 1 is $\sigma_\theta/\theta \approx \pm 0.09$ leading to an error contribution of ±4.5%. For a star of effective temperature 3000K this corresponds to an error in the temperature of about ±160K. Taking a mean bolometric flux relative error of ±15% we obtain a contribution to the effective temperature error of ±3.75%, or approximately ±115K for the star just mentioned.

2. Stellar Radii

We have searched the Hipparcos database at SIMBAD to find stars in our observed sample that have had accurate parallax determinations. Fewer than a half dozen of the stars listed in Table 2 have parallaxes that are less than 3σ above the measurement errors. We have isolated stars classified luminosity class II or II-II from those classified as luminosity class III. Data from these two groups have been plotted in Figure 5 as stellar radius (in solar units) versus effective temperature, where class II and II-III stars are shown as open boxes (☐) and class III stars are shown as filled diamonds (♦). One may see that there is a clear separation between the two luminosity classes with the class II and II-III stars being larger than the class III stars. Around an effective temperature of 3500 K the higher luminosity stars have approximately a factor of two larger radius, on the average, than do the lower luminosity stars.

The principal source of error in Figure 5 is still the error in the parallax. With increased precision in these measurements it should be possible to establish quantitative values of radius corresponding to subtle spectroscopic luminosity differences. In fact, it is this limitation in establishing the distance to our sample of stars that prevents us from constructing an H-R Diagram with the data at hand. While the parallaxes are often 5-10σ results, a level of precision that allows us to see gross radius differences readily, the effect of computing luminosity is to increase the relative error by a factor of two (since distance enters as the second power). This yields an H-R diagram that is not even qualitatively useful.

This research has made use of the SIMBAD database, operated by the CDS, Strasbourg, France. HMD acknowledges support from NSF grant AST-958129 while he was at the University of Wyoming. GTvB was supported while he was a student at the University of Wyoming by a grant from the PASS Center. Portions of this work were performed at the Jet Propulsion Laboratory, California Institute of Technology under contract with the National Aeronautics and Space Administration.

REFERENCES

Carleton, N. P. *et al.* 1994, *Proc. SPIE*, **2200**, 152

DiBenedetto, G. P. & Rabbia, Y. 1987, *A&A*, **188**, 114

DiBenedetto, G. P. & Ferluga, S. 1990, *A&A*, **236**, 449

Dyck, H. M., Benson, J. A. & Ridgway, S. T. 1993, *PASP*, **105**, 610

Dyck, H. M., Benson, J. A., van Belle, G. T. & Ridgway, S. T. 1996, *AJ*, **111**, 1705 (Paper I)

Elias, J. H., Frogel, J. A. & Humphreys, R. M. 1985, *ApJS*, **57**, 91

Hoffleit, D. 1982, *Catalogue of Bright Stars* (Yale University Press, New Haven)

Houk, N. & Smith-Moore, M. 1988, *Michigan Catalogue of Two Dimensional Spectral Types for the HD*, **4** (University of Michigan, Department of Astronomy, Ann Arbor)

Keenan, P. C. 1942, *ApJ*, **95,** 461

Keenan, P. C. 1963, *Basic Astronomical Data*, edited by K. Aa. Strand (University of Chicago Press, Chicago), chapter 8

Keenan, P. C. & McNeil, R. C. 1989, *ApJS*, **71**, 245

Lockwood, G. W. 1972, *ApJS*, **24**, 375

Moore, J. H. & Paddock, G. F. 1950, *ApJ*, **112**, 48

Morgan, W. W. & Keenan, P. C. 1973, *ARAA*, **11**, 29

Perrin, G., Coude du Forresto, V., Ridgway, S. T.,... 1997, Science with the VLT Interferometer, ESO Astrophysics Symposia, F. Paresce, ed. (Springer-Verlag: xxxx), 318-319.

Ridgway, S. T., Joyce, R. R., White, N. M. & Wing, R. F. 1980, *ApJ*, **235**, 126

Tuthill, P. G. 1994, PhD Dissertation, University of Cambridge

White, N. M. & Feierman, B. H. 1987, *AJ*, **94**, 751

Wright, K. O. 1970, *Vistas in Astronomy*, **12**, 147

BS	NAME	YrMoDa	B_p (m)	V	$\theta_{UD} \pm \sigma_0$ (mas)
337	β AND	951005	36.71	0.196	12.2±0.6
603	γ^1 AND	951005	37.06	0.644	7.0±0.6
617	α ARI	951008	38.24	0.722	5.9±0.6
867	RZ ARI	951008	38.25	0.430	9.1±0.5
867	RZ ARI	961004	37.18	0.394	9.8±0.6
911	α CET	951006	33.22	0.328	11.7±0.6
911	α CET	951007	32.86	0.354	11.5±0.6
1155	BE CAM	961006	33.07	0.630	8.1±0.6
1577	ι AUR	951008	38.23	0.694	6.3±0.6
1845	119 TAU	951008	38.26	0.429	9.1±0.5
2091	π AUR	951005	36.63	0.517	8.5±0.6
3576	ρ UMA	960309	32.22	0.758	6.5±0.8
3639	RS CNC	960307	21.20	0.443	16.2±1.0
3705	α LYN	960312	38.24	0.606	7.2±0.6
4057	γ^1 LEO	960310	36.80	0.563	8.0±0.6
4057	γ^1 LEO	960311	36.82	0.537	8.3±0.6
4057	γ^1 LEO	960312	38.13	0.655	6.7±0.6
4362	72 LEO	960312	38.21	0.742	5.7±0.6
4434	λ DRA	960309	31.23	0.721	7.3±0.7

Table 1. The new visibility and uniform disk diameter data.

BS	NAME	YrMoDa	B_p (m)	V	$\theta_{UD} \pm\sigma_\theta$ (mas)
…	IRC+40226	960306	21.16	0.720	10.8±1.1
…	IRC+40226	960312	38.24	0.506	8.3±0.5
4483	ω VIR	960317	34.51	0.730	6.5±0.7
…	RU CRT	960317	32.80	0.673	7.6±0.7
…	Z UMA	960309	32.82	0.704	7.2±0.7
…	BK VIR	960317	33.21	0.375	11.2±0.6
4909	TU CVN	960529	37.43	0.656	6.8±0.6
4910	δ VIR	960317	34.13	0.468	9.8±0.6
4949	40 COM	960310	37.41	0.598	7.5±0.6
4949	40 COM	960311	37.41	0.652	6.9±0.6
4949	40 COM	960312	38.22	0.647	6.8±0.6
4949	40 COM	960602	37.51	0.710	6.2±0.6
5299	BY BOO	960530	37.32	0.636	7.1±0.6
5299	BY BOO	960606	35.50	0.658	7.2±0.6
…	CI BOO	960607	35.38	0.770	5.8±0.7
…	RV BOO	960306	21.20	0.737	10.4±1.1
…	RV BOO	960308	21.20	0.748	10.1±1.1
5512	HD130144	960311	37.02	0.518	8.4±0.6

Table 1. The new visibility and uniform disk diameter data.

BS	NAME	YrMoDa	B_p (m)	V	$\theta_{UD} \pm \sigma_\theta$ (mas)
5512	HD130144	960312	38.13	0.486	8.5±0.5
5563	β UMI	960606	27.69	0.627	9.7±0.8
5589	RR UMI	960606	28.99	0.600	9.6±0.7
5654	FL SER	960602	36.98	0.593	7.6±0.6
…	IRC 00265	960317	34.52	0.667	7.3±0.6
…	IRC 00265	960604	31.59	0.773	6.4±0.8
5879	κ SER	960311	36.69	0.748	5.9±0.7
5879	κ SER	960602	37.30	0.689	6.5±0.6
…	ST HER	960529	36.75	0.420	9.6±0.6
…	ST HER	960530	36.98	0.460	9.1±0.6
…	ST HER	960601	35.64	0.451	9.5±0.6
…	X HER	960601	35.82	0.149	13.1±0.7
6039	LQ HER	960312	38.22	0.704	6.1±0.6
6056	δ OPH	960317	34.13	0.505	9.3±0.6
6086	AT DRA	960601	34.57	0.798	5.5±0.7
…	R UMI	960606	26.64	0.763	7.8±0.9
…	S DRA	960531	35.85	0.681	6.8±0.6
…	S DRA	960601	34.80	0.694	6.9±0.6
6242	V636 HER	960530	37.54	0.758	5.6±0.6

Table 1. The new visibility and uniform disk diameter data.

BS	NAME	YrMoDa	B_p (m)	V	$\theta_{UD} \pm \sigma_\theta$ (mas)
…	IRC+40292	960529	36.83	0.832	4.7±0.8
…	IRC+40292	960607	35.52	0.737	6.2±0.7
…	IRC-10359	960604	30.53	0.795	6.3±0.8
6418	π HER	960529	37.07	0.803	5.1±0.7
6418	π HER	960607	35.51	0.766	5.8±0.7
6702	OP HER	960528	37.23	0.729	6.0±0.6
6705	γ DRA	960601	34.81	0.458	9.7±0.6
6765	98 HER	960312	38.24	0.787	5.1±0.7
…	IQ HER	960312	38.21	0.765	5.4±0.6
…	IQ HER	960602	37.22	0.800	5.1±0.7
…	IQ HER	960606	35.39	0.734	6.3±0.7
…	TU LYR	960607	35.28	0.666	7.1±0.6
…	IRC-10414	960604	29.74	0.780	6.7±0.8
7009	XY LYR	960529	37.37	0.527	8.3±0.6
7139	δ^2 LYR	951008	38.25	0.411	9.3±0.5
7139	δ^2 LYR	960529	37.39	0.310	10.6±0.6
…	T SGE	960602	37.40	0.651	6.9±0.6
…	T SGE	960603	37.19	0.599	7.5±0.6

Table 1. The new visibility and uniform disk diameter data.

BS	NAME	YrMoDa	B_p (m)	V	$\theta_{UD} \pm \sigma_\theta$ (mas)
…	T SGE	960607	35.26	0.496	9.1±0.6
…	CH CYG	961007	37.07	0.336	10.4±0.6
…	AF CYG	960528	36.88	0.745	5.9±0.6
…	IRC+20439	960602	37.38	0.438	9.2±0.5
7635	γ SGE	960603	37.51	0.728	6.0±0.6
7645	VZ SGE	960607	35.48	0.716	6.5±0.7
…	AC CYG	960531	34.61	0.735	6.4±0.7
…	AC CYG	960531	34.94	0.816	5.2±0.8
…	BC CYG	960529	37.33	0.657	6.8±0.6
…	RS DEL	960603	37.34	0.784	5.3±0.6
…	RT DEL	960602	37.41	0.736	5.9±0.6
…	DY VUL	960607	35.34	0.681	6.9±0.6
…	RS CAP	960604	29.33	0.765	7.0±0.8
…	IRC+60305	961006	33.60	0.783	6.9±0.7
…	IRC+50383	960601	34.72	0.750	6.2±0.7
…	RU CYG	951004	35.06	0.526	8.8±0.6
…	RU CYG	951005	35.84	0.558	8.3±0.6
…	RV CYG	951008	38.24	0.577	7.6±0.5

Table 1. The new visibility and uniform disk diameter data.

BS	**NAME**	**YrMoDa**	**B_p (m)**	**V**	**$\theta_{UD} \pm \sigma_{\theta}$ (mas)**
8308	ε PEG	951006	34.30	0.612	8.0±0.6
8308	ε PEG	960603	37.30	0.565	7.9±0.6
…	GY CYG	960531	35.26	0.754	6.0±0.7
…	GY CYG	960601	35.23	0.792	5.5±0.7
8465	ζ CEP	961006	34.05	0.800	5.6±0.8
…	SV CAS	961007	36.28	0.660	7.0±0.6
…	RS AND	961007	36.33	0.629	7.4±0.6
9064	ψ PEG	961004	37.65	0.694	6.4±0.6
9089	30 PSC	951006	33.18	0.694	7.2±0.7
9089	30 PSC	951007	32.93	0.704	7.1±0.7

Table 2. The derived data.

BS	HD	Name	Spectrum	$T_{eff} \pm \sigma_T$ (K)	Ref	F_{bol}(W cm$^{-2}\mu$m^{-1})	$\theta_{UD} \pm \sigma_\theta$(mas)
337	6860	β AND	M0+IIIa	4002±178	KM89	1.33E-12	12.2±0.6
603	12533	γ^1 AND	K3-IIb	4470 ±251	KM89	6.81E-13	7.0±0.6
617	12929	α ARI	K2-IIIab	4790±298	KM89	6.38E-13	5.9±0.6
867	18191	RZ ARI	M6-III	3442±148	KM89	4.32E-13	9.4±0.4
911	18884	α CET	M1.5IIIa	3869±161	KM89	1.05E-12	11.6±0.4
1155	23475	BE CAM	M2+IIab	3550±185	KM89	3.63E-13	8.1±0.6
1577	31398	ι AUR	K3II	4389±263	MK73	5.13E-13	6.3±0.6
1845	36389	119 TAU	M2Iab-Ib	3823±176	KM89	6.16E-13	9.1±0.5
2061	39801	α ORI	M1-2Ia-Ib	3605±43	KM89	1.15E-11	44.2±0.2
2091	40239	π AUR	M3II	3736±190	KM89	4.90E-13	8.5±0.6
3576	76827	ρ UMA	M3IIIb	3279±233	KM89	1.70E-13	6.5±0.8

Table 2. The derived data.

BS	HD	Name	Spectrum	$T_{eff}\pm\sigma_T$ (K)	Ref	F_{bol}(W $cm^{-2}\mu m^{-1}$)	$\theta_{UD}\pm\sigma_\theta$(mas)
3639	78712	RS CNC	M6IIIase	3120±126	BSC	8.47E-13	16.0±0.5
3705	80493	α LYN	K7IIIab	3969±220	KM89	4.48E-13	7.2±0.6
4057	89484	γ^1 LEO	K1-IIIb	3949±172	KM89	4.98E-13	7.7±0.3
4362	97778	72 LEO	M3IIb	3734±238	KM89	2.20E-13	5.7±0.6
4434	100029	λ DRA	M0III	3526±212	KM89	2.87E-13	7.3±0.7
4483	101153	ω VIR	M4-4.5III	3544±229	K63	2.32E-13	6.5±0.7
....	103681	Z UMA	M5IIIvar	2596±157	K42	8.20E-14	7.2±0.7
....	108849	BK VIR	M7-III:	3074±141	KM89	3.90E-13	11.2±0.6
4909	112264	TU CVN	M5-III	3350±159	KM89	2.21E-13	7.1±0.4
4910	112300	δ VIR	M3+III	3783±182	KM89	6.85E-13	9.8±0.6
4949	113866	40 COM	M5III	3433±148	BSC	2.27E-13	6.8±0.3

Table 2. The derived data.

BS	HD	Name	Spectrum	$T_{eff} \pm \sigma_T$ (K)	Ref	F_{bol}(W cm$^{-2}\mu$m^{-1})	$\theta_{UD} \pm \sigma_\theta$(mas)
5299	123657	BY BOO	M4.5III	3506±147	KM89	2.55E-13	7.0±0.3
5340	124897	α BOO	K1.5III	4628±210	KM89	5.83E-12	19.1±1.0
....	126009	CI BOO	M3II	3227±226	BSC	1.27E-13	5.8±0.7
....	126327	RX BOO	M7.5-8	2915±113	KM89	8.85E-13	18.8±0.4
5512	130144	.....	M5IIIab	3577±147	BSC	3.82E-13	8.2±0.3
5563	131873	β UMI	K4-III	4086±225	KM89	9.13E-13	9.7±0.8
5589	132813	RR UMI	M4.5III	3464±179	KM89	4.62E-13	9.6±0.7
5654	134943	FL SER	M4IIIab	2830±152	BSC	1.29E-13	7.6±0.6
....	139216	τ^4 SER	M5IIIa	3315±135	KM89	4.20E-13	10.0±0.3
5879	141477	κ SER	M0.5IIIab	3575±185	KM89	2.22E-13	6.2±0.5
....	142143	ST HER	M6-7III(S)	3319±131	KM89	3.72E-13	9.4±0.2

Table 2. The derived data.

BS	HD	Name	Spectrum	$T_{eff}\pm\sigma_T$ (K)	Ref	F_{bol}(W $cm^{-2}\mu m^{-1}$)	$\theta_{UD}\pm\sigma_\theta$(mas)
....	144205	X HER	M7	3281±130	L72	6.05E-13	12.2±0.3
6039	145713	LQ HER	M4.5IIIa	3457±211	BSC	1.85E-13	6.1±0.6
6056	146051	δ OPH	M0.5III	3987±168	KM89	7.58E-13	9.3±0.4
6086	147232	AT DRA	M4IIIa	3740±272	BSC	2.06E-13	5.5±0.7
6146	148783	g HER	M6-III	3449±141	KM89	1.08E-12	14.8±0.5
6242	151732	V636 HER	M4.5III	3182±205	KM89	1.12E-13	5.6±0.6
6406	156014	α^1 HER	M5Ib-II	3271±46	KM89	4.34E-12	33.0±0.5
6418	156283	π HER	K3II	4106±239	KM89	2.94E-13	5.4±0.5
6702	163990	OP HER	M5IIb-IIIa	3497±175	K63	1.64E-13	5.6±0.4
6705	164058	γ DRA	K5III	4095±163	KM89	9.06E-13	9.6±0.3
6765	165625	98 HER	M3- S III	3755±289	KM89	1.80E-13	5.1±0.7

Table 2. The derived data.

BS	HD	Name	Spectrum	$T_{eff}\pm\sigma_T$ (K)	Ref	F_{bol}(W cm$^{-2}\mu$m^{-1})	$\theta_{UD}\pm\sigma_\theta$(mas)
....	168198	IQ HER	M4II-M6III	3502±176	BSC	1.63E-13	5.6±0.4
7009	172380	XY LYR	M4.5-5+II	3351±143	KM89	2.26E-13	7.2±0.3
7139	175588	δ^2 LYR	M4II	3637±145	KM89	5.79E-13	9.7±0.3
7157	175865	R LYR	M5III	3749±164	BSC	1.23E-12	13.4±0.6
....	182917	CH CYG	M7IIIvar	3084±130	APJ45	3.15E-13	10.0±0.4
7525	186791	γ AQL	K3II	4106±174	KM89	5.53E-13	7.5±0.3
7536	187076	δ SGE	M2II	3779±164	BSC	4.32E-13	7.8±0.3
7635	189319	γ SGE	M0-III	4189±238	KM89	3.24E-13	5.5±0.5
7645	189577	VZ SGE	M4IIIa	3844±251	BSC	2.30E-13	5.5±0.6
7735	192577	31 CYG	K4Ib	3466±216	W70	1.75E-13	5.9±0.6
7751	192909	32 CYG	K5Iab	3543±214	W70	2.11E-13	6.2±0.6

Table 2. The derived data.

BS	HD	Name	Spectrum	$T_{eff} \pm \sigma_T$ (K)	Ref	F_{bol}(W $cm^{-2} \mu m^{-1}$)	$\theta_{UD} \pm \sigma_\theta$(mas)
....	......	BC CYG	M4Ia	3673±210	EFH85	2.93E-13	6.8±0.6
7886	196610	EU DEL	M6III	3508±145	KM89	5.03E-13	9.8±0.3
7941	197812	U DEL	M5II-III	3389±155	BSC	2.83E-13	7.8±0.4
7951	198026	EN AQR	M3III	3933±286	KM89	2.52E-13	5.5±0.7
8079	200905	ξ CYG	K4.5Ib-II	3491±189	KM89	2.91E-13	7.5±0.6
....	200994	RS CAP	M6-7III	3469±234	MSS88	2.47E-13	7.0±0.8
....	202380	IRC+60305	M2Ib	3774±261	KM89	2.46E-13	5.9±0.7
....	203712	V1070 CYG	M7III	3526±164	MP50	3.07E-13	7.6±0.4
8262	205730	W CYG	M5IIIae	3373±143	BSC	5.88E-13	11.4±0.5
8308	206778	ε PEG	K2Ib-II	4459±184	KM89	7.83E-13	7.5±0.3
8465	210745	ζ CEP	K1.5Ib	4246±337	KM89	3.55E-13	5.6±0.8

Table 2. The derived data.

BS	**HD**	**Name**	**Spectrum**	**$T_{eff}\pm\sigma_T$ (K)**	**Ref**	**F_{bol}(W cm$^{-2}\mu$m^{-1})**	**$\theta_{UD}\pm\sigma_\theta$(mas)**
8698	216386	λ AQR	M2.5III	3477±187	KM89	4.03E-13	8.9±0.7
8775	217906	β PEG	M2.5II-III	3890±174	KM89	1.63E-12	14.3±0.7
9064	224427	ψ PEG	M3III	3475±206	KM89	2.08E-13	6.4±0.6
9089	224935	30 PSC	M3III	3647±184	KM89	3.15E-13	7.2±0.5

References to Table 2: KM89 = Keenan & McNeil (1989), BSC = Hoffleit (1982), MK73 = Morgan & Keenan (1973), K63 = Keenan (1963), K42 = Keenan (1942), L72 = Lockwood (1972), APJ45 = Keenan & Hynek (1945), W70 = Wright (1970), EFH85 = Elias, Frogel & Humphreys (1985), MSS88 = Houk & Smith-Moore (1988), MP50 = Moore & Paddock (1950).

FIGURE CAPTIONS

Figure 1. A plot of the 2.2μm visibility data for the M5 supergiant α^1 Her with a Uniform Disk visibility function plotted for comparison. Note that there is no apparent systematic difference between the observations and the simple model for this atmospherically-extended star. This is used as justification for deriving the angular diameter for giants and supergiants from a single observation of the visibility at one spatial frequency point.

Figure 2. A comparison of the uniform disk angular diameter (UDD) observations made at IOTA with those obtained by other means. Sources for the other measurements are discussed in the text. The line shown in the figure is the best fit to the data and is also discussed in the text.

Figure 3. A plot of the absolute visibility deviation versus visibility for all stars measured in this paper and in Paper I that have observations on two or more nights. Note that there is no change of the scatter with observed visibility. See the text for a more detailed explanation.

Figure 4. A plot of the effective temperature versus spectral type for luminosity classes II, II-III and III stars, comparing the results of lunar occultation observations with those from interferometry, all made at near-infrared wavelengths. The dashed line is a linear regression discussed in the text.

Figure 5. A plot of stellar radius as a function of effective temperature. Note that luminosity class II and II-III stars are systematically larger than luminosity class III stars at a given effective temperature.

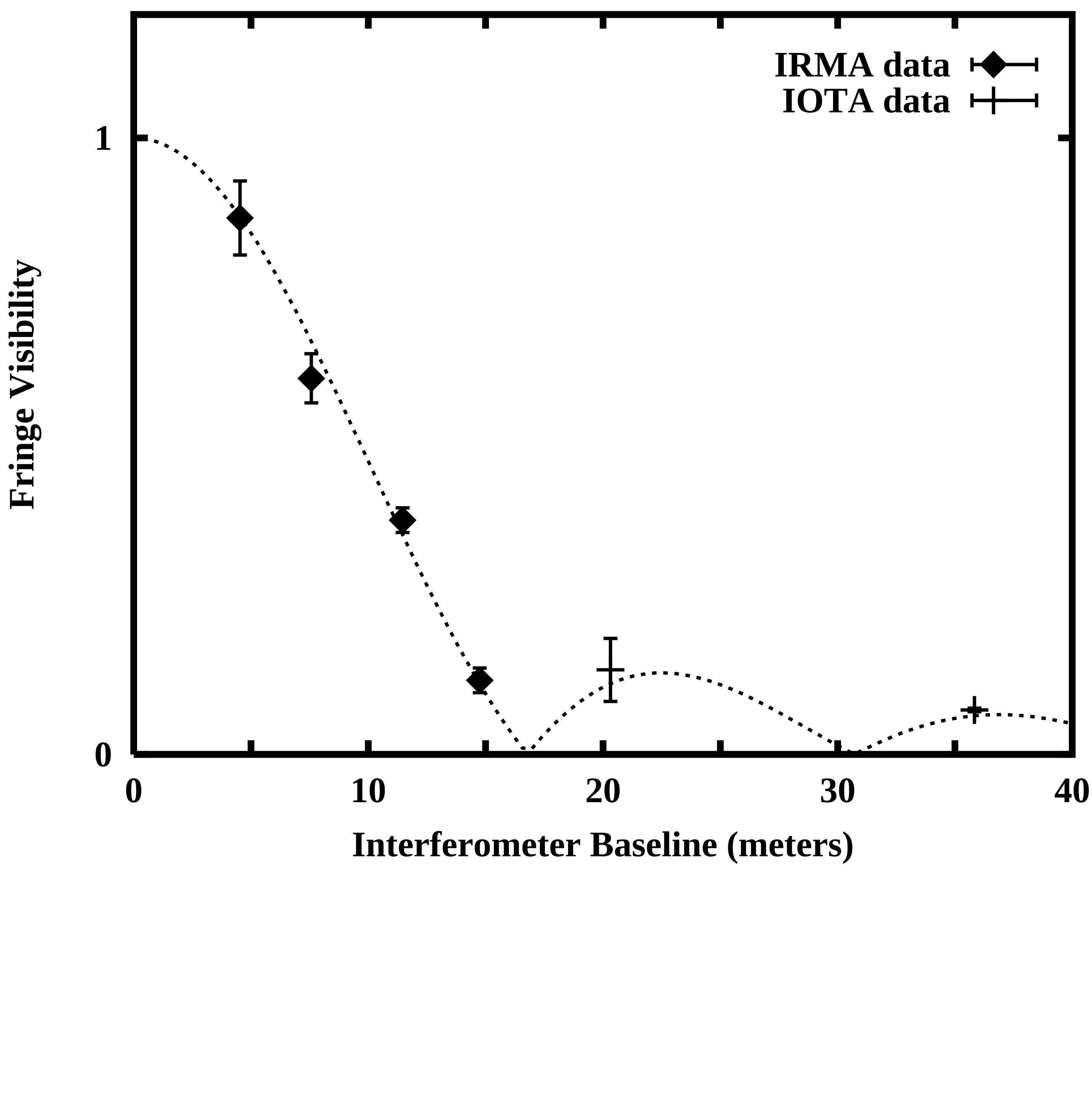

IRMA data
IOTA data
1
0
Fringe Visibility
0
10
20
30
40
Interferometer Baseline (meters)

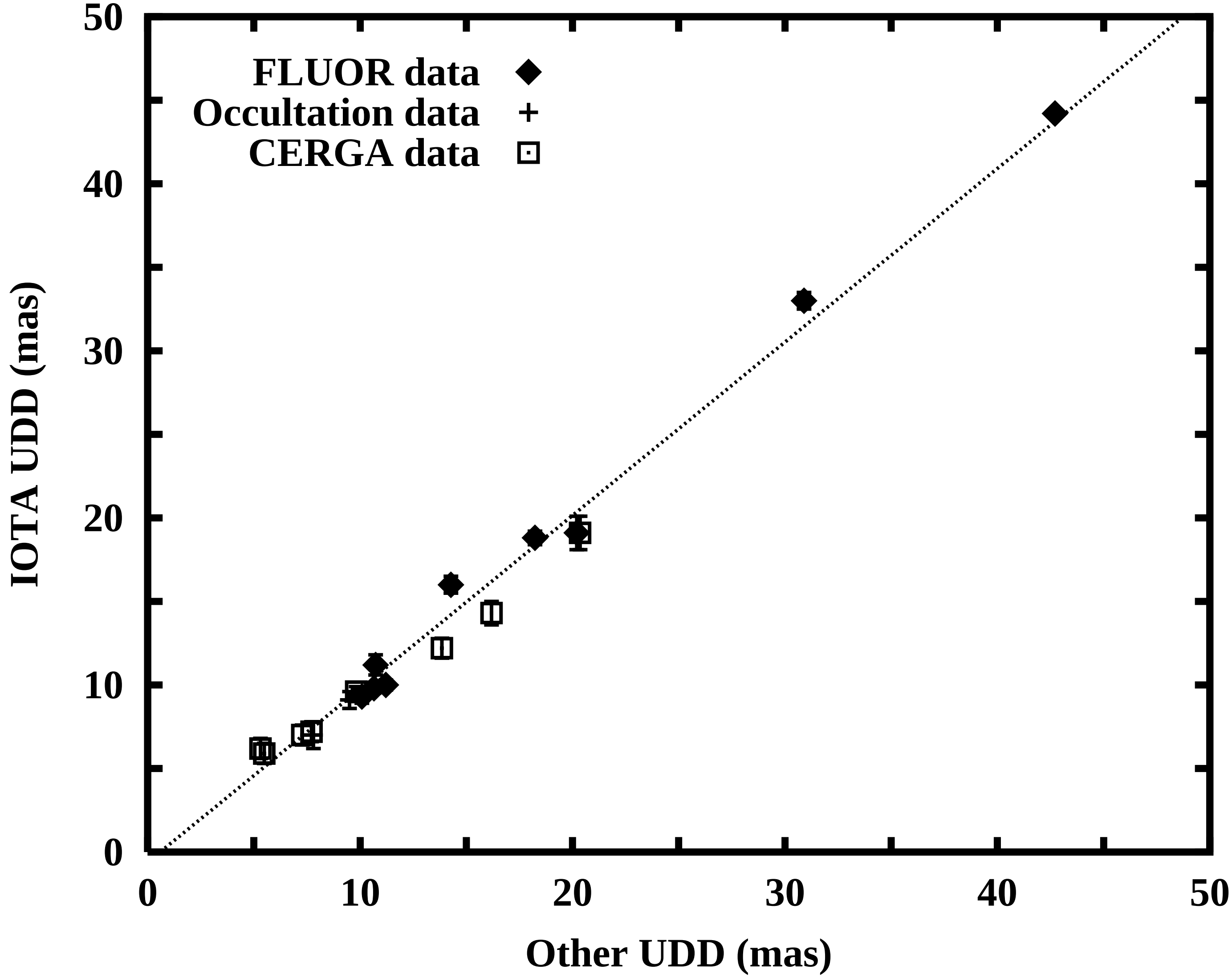

FLUOR data
Occultation data
CERGA data
IOTA UDD (mas)
Other UDD (mas)
0
10
20
30
40
50
0
10
20
30
40
50

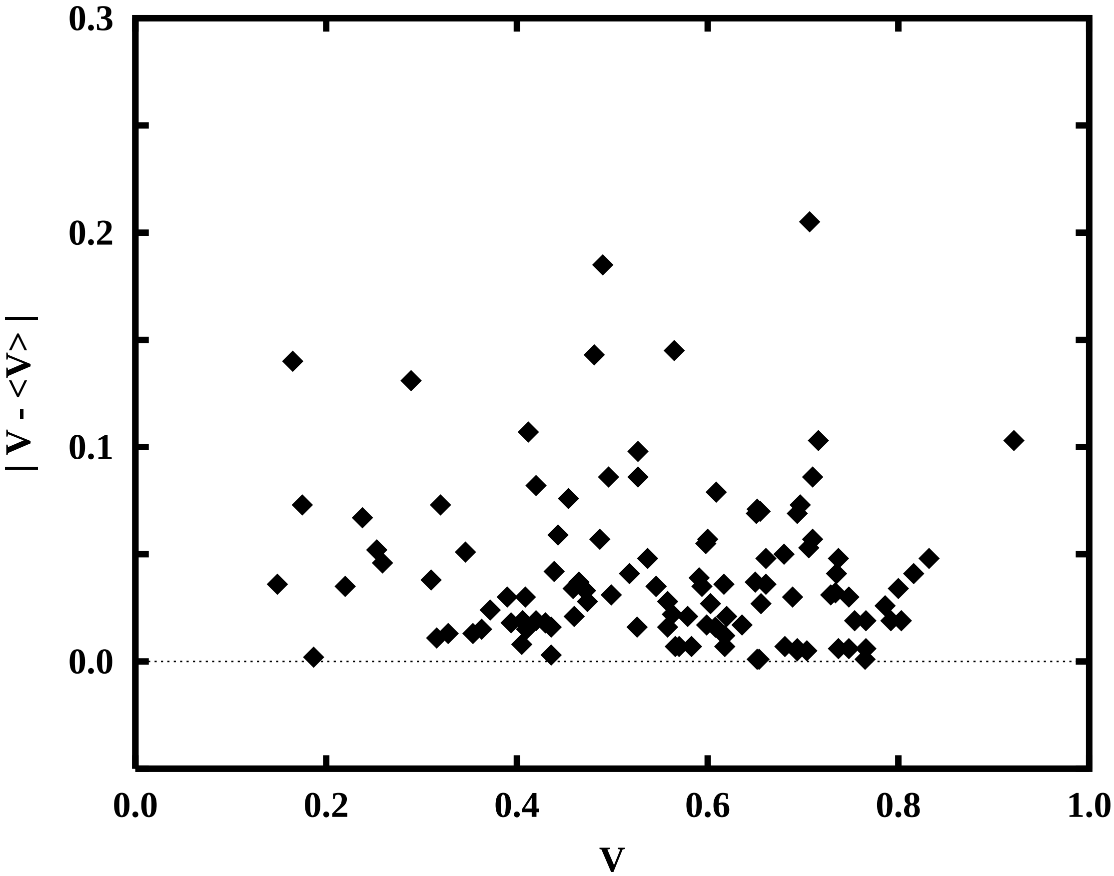

0.3
0.2
0.1
0.0
| V - <V> |
0.0
0.2
0.4
0.6
0.8
1.0
V

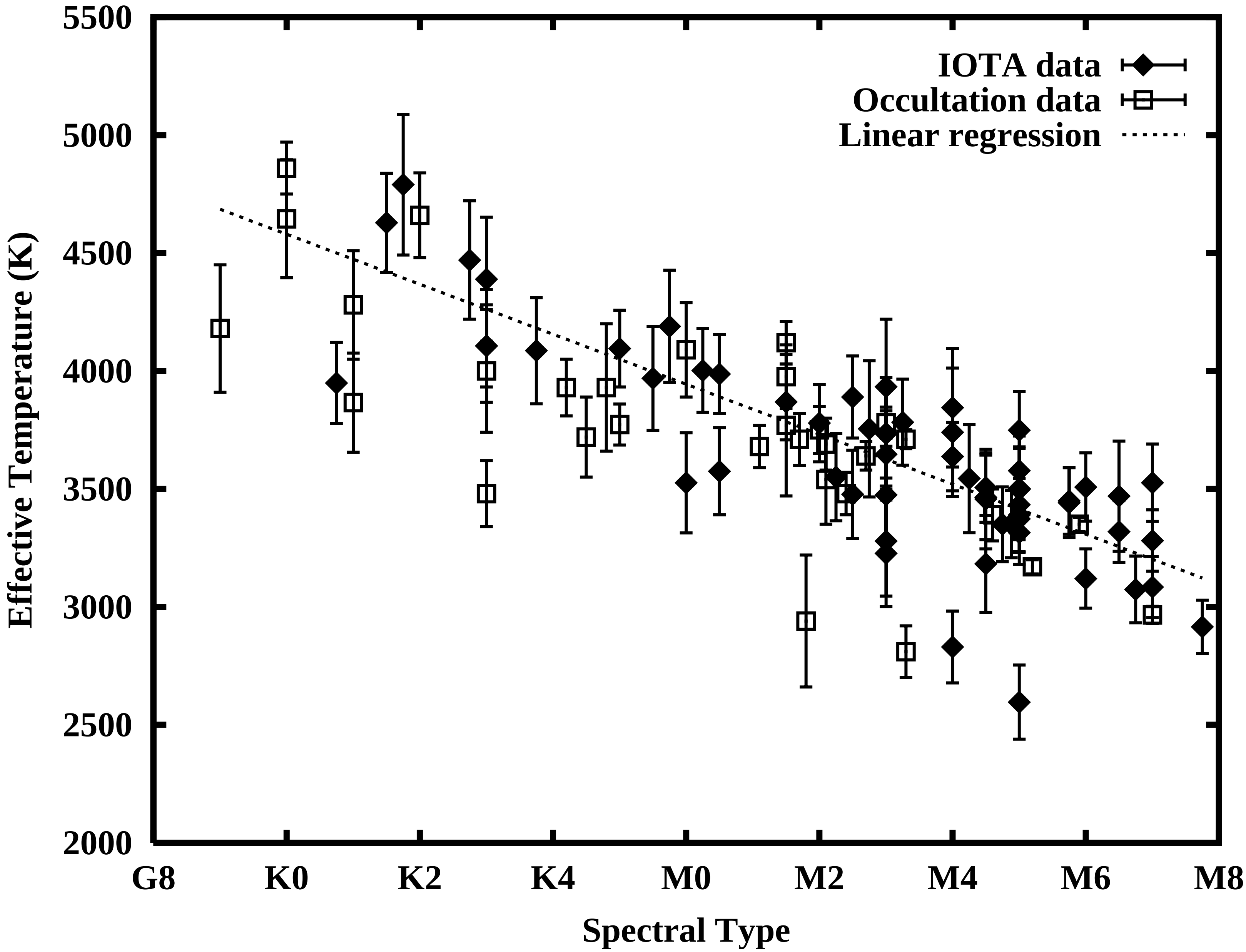

IOTA data
Occultation data
Linear regression
5500
5000
4500
4000
3500
3000
2500
2000
Effective Temperature (K)
G8
K0
K2
K4
M0
M2
M4
M6
M8
Spectral Type

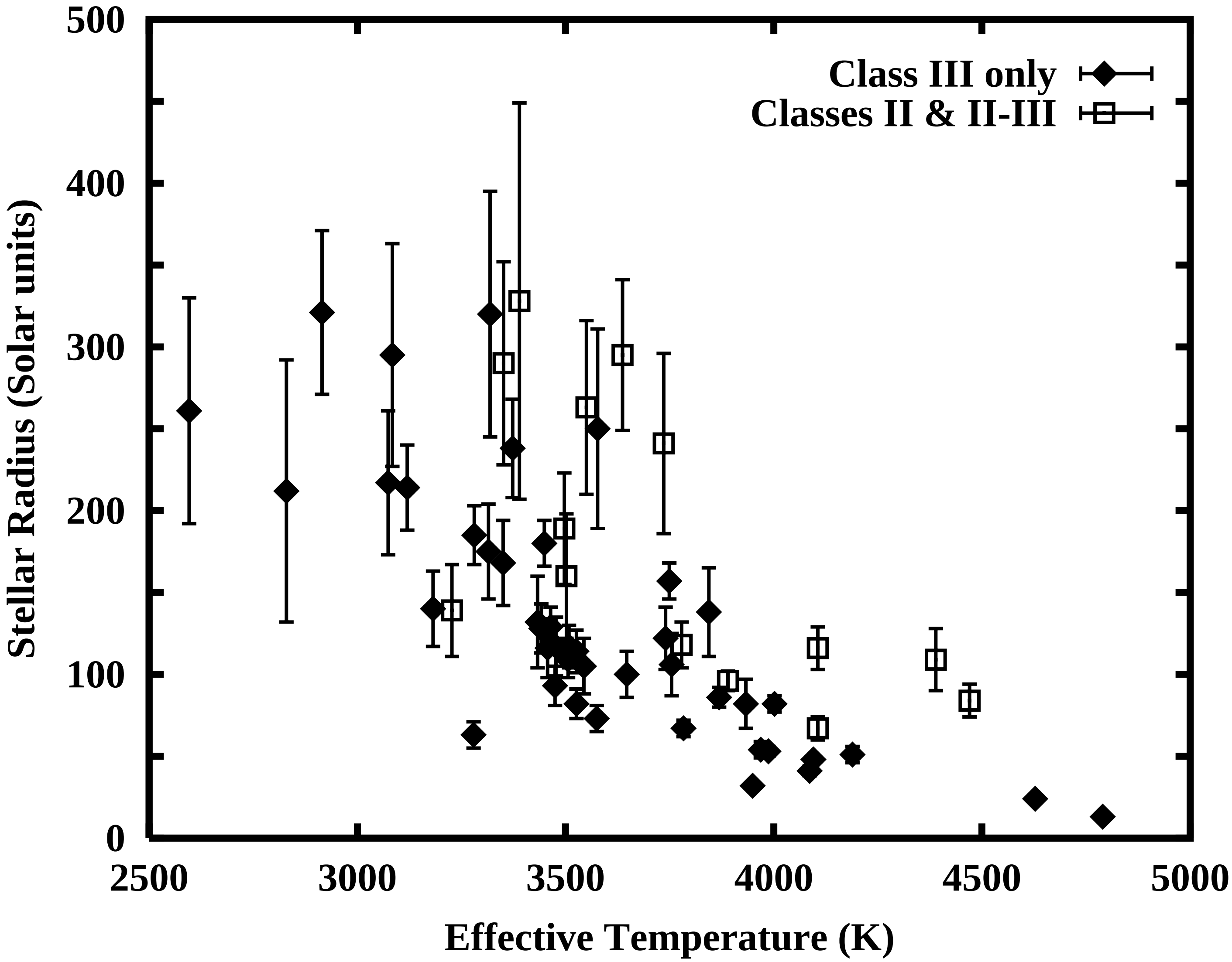
Class III only
Classes II & II-III
Stellar Radius (Solar units)
Effective Temperature (K)
0
100
200
300
400
500
2500
3000
3500
4000
4500
5000